Journal of Alloys and Compounds 509S (2011) S625–S628

Contents lists available at ScienceDirect

Journal of Alloys and Compounds

journal homepage: www.elsevier.com/locate/jallcom

Hydrogen storage properties of compacts of melt-spun $Mg_{90}Ni_{10}$ flakes and expanded natural graphite

Carsten Pohlmann[a], Lars Röntzsch[b,*], Siarhei Kalinichenka[a], Thomas Hutsch[b], Thomas Weißgärber[b], Bernd Kieback[a,b]

[a] Institute for Materials Science, Dresden University of Technology, Helmholtzstraße 7, 01069 Dresden, Germany
[b] Fraunhofer Institute for Manufacturing Technology and Applied Materials Research IFAM, Winterbergstraße 28, 01277 Dresden, Germany

ARTICLE INFO

Article history:
Received 22 July 2010
Received in revised form 9 November 2010
Accepted 10 November 2010
Available online 18 November 2010

Keywords:
Hydrogen storage material
Metal hydrides
Magnesium alloy
Melt spinning
Heat conductivity
Hydride graphite composite
Expanded natural graphite

ABSTRACT

In recent years, melt-spun magnesium alloys have attracted a lot of attention due to their excellent (de-)hydrogenation characteristics resulting from their nanoscale crystal structure and the homogeneous distribution of minor catalyst phases. Besides reaction kinetics, the heat conductivity of the storage material is important to transfer the reaction enthalpies in a controlled manner. Due to the inferior heat conduction properties of magnesium hydride, composites containing melt-spun $Mg_{90}Ni_{10}$ flakes and expanded natural graphite (ENG) up to 25.5 wt.% have been examined. Mixtures of those starting materials were compacted to cylindrical pellets using compaction pressures up to 600 MPa. Investigations of thermal conductivities in radial and axial directions, microstructure and phase fractions were carried out upon all sets of specimens. The heat transfer characteristics were tuned in a wide range from 1 up to 47 $W\,m^{-1}\,K^{-1}$. Furthermore, cyclic (de-)hydrogenation was carried out upon the compacts showing a hydrogen uptake of up to 4 wt.%-H_2 within 10 min. During the hydrogen loading process, the $Mg_{90}Ni_{10}$–ENG pellets remained mechanically stable.

1. Introduction

In recent years, the (de-)hydrogenation kinetics of magnesium-based systems have been enhanced steadily by producing nano-scale microstructures and by adding catalytically active constituents (e.g. transition metals, metal oxides, rare earth elements or carbon-based additives) [1–5]. Another approach considering hydride-based hydrogen storage systems is the improvement of the heat transfer characteristics of the commonly granular hydrogen storage material, especially in its hydrogenated state. Thereby, the storage tank's (un-)loading dynamics can be controlled, too. A few studies were conducted to improve the rather poor thermal conductivity of MgH_2 of less than 1 $W\,m^{-1}\,K^{-1}$, which can be divided into two groups: At first, supplementary metallic structures were used with high thermal conductivity like nickel or aluminium foams [6–8]. Secondly, the preparation of hydride–graphite composites was pursued with increased effective thermal conductivity [9–12]. Accurate tailoring of the thermal conductivity and creating anisotropic heat conduction properties can be achieved by the latter method. For example, Chaise et al. [9] increased the effective thermal conductivity of compacts of magnesium hydride and 10 wt.% expanded natural graphite (ENG) to about 8 $W\,m^{-1}\,K^{-1}$ in the direction of ENG alignment.

As demonstrated in our previous publications, melt spinning allows to produce nanoscale microstructures of Mg–Ni and Mg–Ni–Y alloys with gravimetric hydrogen storage capacities of up to 5.5 wt.%-H_2 and hydrogen uptake rates of up to 1.3 wt.%-H_2 per minute [13,14]. Considering the well known catalytic effect of Nickel upon hydrogenation of magnesium [15–17], a melt-spun magnesium–nickel alloy ($Mg_{90}Ni_{10}$) is used in this work as starting material to produce $Mg_{90}Ni_{10}$–ENG composites with ENG contents of up to 25.5 wt.%. Furthermore, the tank architecture sets essential requirements upon the heat flux inside the storage material. In this regard, a reasonable design, which can be found in various publications [8,18–21], is a cylindrical geometry where the heat flux needs to be transported only in radial direction. In order to reach acceptable hydrogen loading times in the range of 1 wt.%-H_2 per minute the effective heat conductivity within the hydrogen storage material should be in the range from 10 to 20 $W\,m^{-1}\,K^{-1}$ in radial direction according to our approximate calculations.

In this contribution, it is demonstrated that the radial thermal conductivity of cylindrical $Mg_{90}Ni_{10}$–ENG compacts can be tailored in a wide range. Further, it is shown for the first time that the compacts can be hydrogenated while keeping their mechanical sta-

* Corresponding author. Tel.: +49 351 2537 411; fax: +49 351 2537 399.
E-mail address: Lars.Roentzsch@ifam-dd.fraunhofer.de (L. Röntzsch).

0925-8388/$ – see front matter © 2010 Elsevier B.V. All rights reserved.
doi:10.1016/j.jallcom.2010.11.060

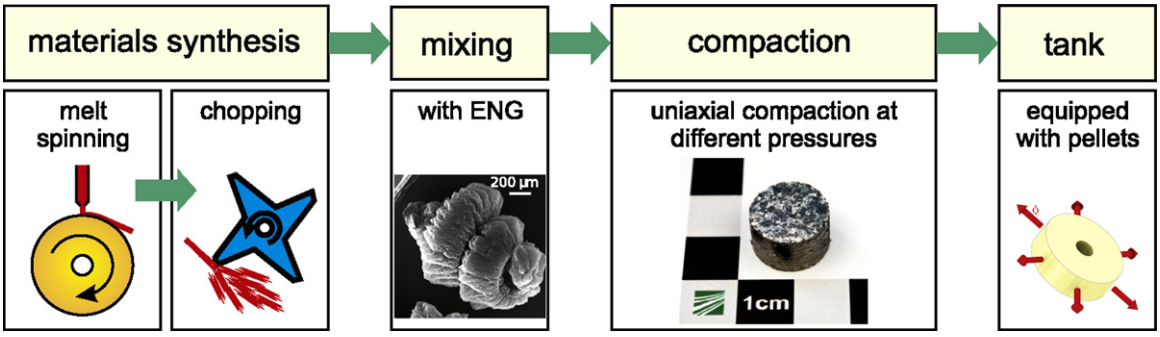

Fig. 1. Schematic technology chain of the production of melt-spun magnesium–ENG compacts.

bility. Additionally, we present a technology chain which shows the technical feasibility of the production of the hydride–graphite pellets which are to be used in the cylindrical tank system.

2. Experimental

The initial metallic state of $Mg_{90}Ni_{10}$ was prepared by melt spinning. For this purpose, $Mg_{90}Ni_{10}$ master alloy ingots were produced by induction melting of a mixture of pure Mg metal (99.9% purity) and Ni powder (99.9% purity) in a tantalum crucible under argon atmosphere. Melt spinning of this master alloy was then carried out under argon atmosphere. The resulting $Mg_{90}Ni_{10}$ ribbons were 40 μm in thickness and 10 mm in width (cf. [13]).

For further materials manufacturing, a powder metallurgical technology chain was followed, which schematically is depicted in Fig. 1. The melt-spun $Mg_{90}Ni_{10}$ ribbons were repeatedly chopped (Retsch SM 2000) until a maximum flake size of about 1 mm was reached. Afterwards, mixtures of $Mg_{90}Ni_{10}$ flakes with three different ENG (delivered by SGL Carbon) contents of 5.0, 10.0 and 25.5 wt.% were produced using a tubular mixer. After mixing, the $Mg_{90}Ni_{10}$–ENG blend was consolidated by uniaxial compaction (TIRA test 2300) into cylindrical pellets with 14 mm in diameter. Three different compaction pressures, 150, 300 and 600 MPa, were applied. A future tank construction can be equipped with similar prepared pellets which can be larger in diameter and possibly ring shaped.

The geometric density of the pellets was determined. Thereby, the residual porosity within the specimen was calculated by comparison of the pellets' densities with their theoretical bulk densities. The densities of the bulk materials were measured with a pycnometer on single phase pellets (AccuPyc 1330). Inaccuracies of the weight measurements conducted are negligibly small since the systematic error of the used microbalance is less than 0.05 mg. Concerning the measurements of the pellet dimensions (diameter, height), the error of the micrometer caliper employed amounts to 0.004 mm.

In order to distinguish the thermal conductivity in axial and radial direction, the pellets were cut into two 2 mm thin slices (using an Accutom 5), which were orientated parallel and perpendicular to the direction of compression. The slices were examined using the flash method (Netzsch LFA 447 NanoFlash) determining temperature diffusivity with an uncertainty of 3% (value given by the manufacturer). The corresponding thermal conductivity was calculated by multiplying temperature diffusivity, density and specific heat capacity. The specific heat capacity was determined using the DSC method (Netzsch DSC 204 F1 Phoenix) with an uncertainty of 3% (value given by the manufacturer). The summation of the major measurement errors results in an uncertainty of about 10% for the thermal conductivities stated. Furthermore, axial and radial cross-sections of each specimen were prepared for metallographic examination (optical and scanning electron microscopy (SEM)).

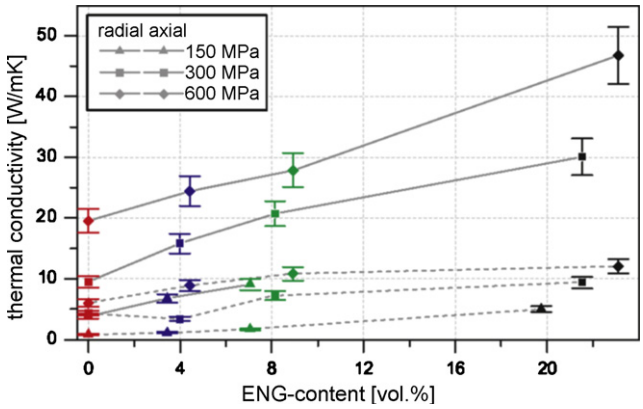

Fig. 2. Radial (solid line) and axial (dashed line) thermal conductivities of the $Mg_{90}Ni_{10}$–ENG compacts at compaction pressures of 150, 300 and 600 MPa vs. ENG content (0 wt.% red, 5 wt.% blue, 10 wt.% green, 25.5 wt.% black). (For interpretation of the references to color in this figure legend, the reader is referred to the web version of the article.)

In order to investigate the stability of the $Mg_{90}Ni_{10}$–ENG pellets during cyclic (de-)hydrogenation, a pellet was placed in a special container in order to set geometrical constraints as it would be the case in a realistic tank (cf. inclusion in Fig. 4). The measurement was performed by thermogravimetry (TG) using a magnetic suspension balance (Rubotherm). The thermal activation of the pellet was achieved during three cycles at 385 °C and pressures between 2 and 30 bar H_2 (99.9998% purity) for 10 h.

3. Results and discussion

As demonstrated in our previous work, the mean porosities of $Mg_{90}Ni_{10}$–ENG pellets are decreasing with increasing compaction pressure [22]. The porosity is reduced with increased ENG content leading to a good compactibility due to the fact that ENG acts as lubricant. The porosity within the $Mg_{90}Ni_{10}$–ENG pellets can be

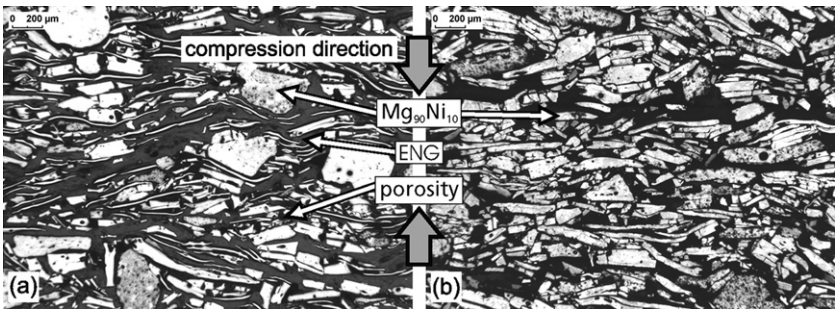

Fig. 3. Optical micrographs of the $Mg_{90}Ni_{10}$–ENG compacts containing (a) 25.5 wt.% and (b) 5.0 wt.% ENG both compacted at 150 MPa (arrows indicating compression direction).

adjusted which allows sufficient hydrogen flow through the compacts and which serves as buffer volume during hydrogenation.

Fig. 2 shows the thermal conductivity of $Mg_{90}Ni_{10}$–ENG pellets. Due to the fact that the effective thermal conductivity of a multi-component material is determined on the basis of the respective volume fractions, the ENG content is given in volume percent of the porous compact. Since the porosity decreases with increasing compaction pressure, the ENG volume fraction slightly increases. For example, the specimens with a ENG content of 10 wt.% have an ENG volume fraction from 7 to 9 vol.% for compaction pressures from 150 to 600 MPa, respectively. Evidently, the thermal conductivity of the cylindrical specimens shows a high degree of anisotropy regarding the heat flow perpendicular (radial) or parallel (axial) to the direction of compaction (cf. Fig. 2). For the applied compaction pressures the axial thermal conductivities cover a narrow range from 0.8 to 11.6 $W\,m^{-1}\,K^{-1}$ with increasing ENG content. On the contrary, a much higher increase of the thermal conductivity in radial direction with increasing ENG content is observed: the thermal conductivity increases from 3.8 to 9.1 $W\,m^{-1}\,K^{-1}$, from 9.5 to 30.1 $W\,m^{-1}\,K^{-1}$ and from 19.5 to 46.7 $W\,m^{-1}\,K^{-1}$ for 150, 300 and 600 MPa compaction pressures, respectively. Furthermore, essential differences at constant ENG content are obvious. For example, the radial thermal conductivity varies between 6.5 $W\,m^{-1}\,K^{-1}$ and 23.4 $W\,m^{-1}\,K^{-1}$ at an ENG content of 5 wt.%. This exemplifies the high influence of the remaining porosity onto the thermal conductivity. Thus, ENG content and compaction pressure are suitable control parameters to tune the thermal conductivity properties in a wide range including the before stated target range from 10 to 20 $W\,m^{-1}\,K^{-1}$ in radial direction.

The above stated anisotropic characteristics in thermal conductivity are further supported by the microstructural examination (cf. Fig. 3). Apparently, ENG as well as the $Mg_{90}Ni_{10}$ flakes is mostly aligned perpendicular to the compression direction which causes the anisotropic heat conduction properties. Fig. 3 shows two examples of optical micrographs of specimens with 25.5 and 5 wt.% ENG for 150 MPa compaction pressure, respectively. Note, that the black domains in Fig. 3(b) represent the ENG phase as well as the residual porosity within the pellets. The comparison between Figs. 3(a) and (b) reveals that the misalignment of the $Mg_{90}Ni_{10}$ flakes increases with increasing ENG content which can be explained by the fact that the flakes can move more freely at higher ENG contents during compaction within the lubricious ENG matrix. At an ENG content of 5 wt.% the $Mg_{90}Ni_{10}$ flakes are collectively aligned in radial direction where the ENG is intercalated. Due to the superior heat conductivity of ENG over $Mg_{90}Ni_{10}$, a percolated network of ENG leads to a higher effective thermal conductivity of the 25.5 wt.% ENG containing composite. A more detailed evaluation of the ENG-induced enhancement is reported elsewhere [22].

Besides heat conduction issues, it is of further importance to ensure that the magnesium alloy–ENG compacts remain dimensionally stable throughout cyclic (de-)hydrogenation. Two facts are important for choosing the right pellet for hydrogenation: At first, it needs to have some porosity to buffer volume expansion during hydrogenation. Secondly, the above stated target value for the thermal conductivity needs to be met. From previous results concerning expected thermal conductivity in its hydrogenated state [22] and its porosity (about 25 vol.%), a pellet with 10 wt.% ENG compacted at 300 MPa was chosen to be cycled for 13 times leaving it in the hydrogenated state. Throughout processing, the pellet remained in its cylindrical shape (cf. inclusion in Fig. 4), due to the special sample container no radial expansion occurred. However, a few plane cracks perpendicular to the direction of compaction were observed which go along with a slight axial expansion of the pellet of about 15%. Nevertheless, considering the earlier mentioned tank architecture where the heat flows in radial direction, suchlike plane cracks do not affect the heat conduction of the overall tank. Therefore, it

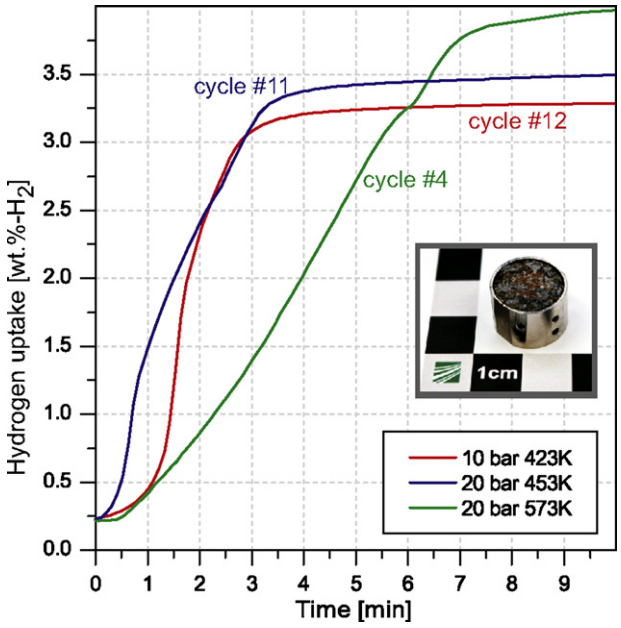

Fig. 4. Hydrogen uptake curve at different temperatures (423 K, 453 K and 573 K) and absorption pressures (10 and 20 bar H_2) of a $Mg_{90}Ni_{10}$ pellet containing 10 wt.% ENG compacted at 300 MPa. Inclusion: $Mg_{90}Ni_{10}$ pellet inside a special container in order to prevent dimensional changes during (de-)hydrogenation.

is expected that the hydrogen uptake dynamics are deteriorated only slightly. In this regard, Fig. 4 depicts the hydrogen absorption of three cycles at different pressures and temperatures supporting this assumption. Apparently, even with 10 wt.% ENG as non-active hydrogen storage material, a reversible hydrogen capacity of about 4 wt.%-H_2 (equals to about 64–72 g-H_2/l) can be reached within 10 min. However, metallography revealed a residual metallic phase within the final pellet which implies an insufficient activation process during the first three cycles. This explains the improvement in sorption kinetics with cycle number (higher slope of hydrogen uptake curves of 0.5, 0.9 and 1.2 m.%-H_2/min for the 4th, 11th and 12th cycle, respectively, cf. Fig. 4). Thus, the activation process needs to be adjusted accordingly.

Overall, the here presented technology chain (as depicted in Fig. 1) has proven to be a feasible way of producing a Mg-based hydrogen storage material starting with melt spinning of its metallic state, admixing with ENG and compacting to pellets. However, volume differences of the metallic compared to the hydrogenated state might cause changes of the alignment of the phases which would thereby influence the effective thermal conductivity of the pellet. For that reason, future research and materials engineering will concentrate on the relationship between thermal conductivity and microstructure as a function of the number of hydrogenation/dehydrogenation cycles.

4. Conclusion

Produced on the basis of a 4-step technology chain, compacts of a composite material consisting of melt-spun $Mg_{90}Ni_{10}$ and ENG were investigated regarding thermal conductivity, microstructure and cyclic (de-)hydrogenation. Four different ENG contents of 0, 5.0, 10.0 and 25.5 wt.% were used at compaction pressures of 150, 300 and 600 MPa. It was presented that ENG strongly improves the heat conduction properties of $Mg_{90}Ni_{10}$ up to 47 $W\,m^{-1}\,K^{-1}$. Furthermore, a strong anisotropy in thermal conductivity of the compacts was found with strongest enhancement perpendicular to the direction of compaction. Microstructural examination showed

both $Mg_{90}Ni_{10}$ flakes and graphite planes are preferably oriented in radial direction being responsible for this strong anisotropy.

Furthermore, the findings illustrate a strong influence of the residual porosity on the effective thermal conductivity of the $Mg_{90}Ni_{10}$–ENG compacts. Apparently, ENG acts as lubricant during compaction which leads to a good compressibility. Exemplarily at a compaction pressure of 600 MPa the residual porosity can be as small as about 10 vol.%. With the major processing parameters (ENG-content and compaction pressure) it is possible to tune thermal conductivity as well as porosity and, thereby, achieving a pellet with tailored properties, i.e. a pellet with a volume fraction of porosity required to buffer expansion during hydrogenation together with a high enough ENG content to give sufficient thermal conductivity.

The hydrogenation of $Mg_{90}Ni_{10}$–ENG compacts does not cause a change in the initial cylindrical shape as cyclic (de-)hydrogenation experiments have shown. However, a small volume expansion of about 15% in axial direction was observed which also leads to small plane cracks perpendicular to the direction of compaction. The hydrogen uptake reached up to 4 wt.%-H_2 within 10 min at a pressure of 20 bar and a temperature of 453 K. Thus, it is shown that suchlike prepared pellets are suitable for hydrogen storage applications in principle. The impacts of the pellet properties (e.g. porosity, ENG phase fraction, and activation process), however, have to be investigated further to obtain an optimal pellet configuration for a cylindrical tank architecture.

Acknowledgements

This work has been performed in the framework of the European Centre for Emerging Materials and Processes Dresden (ECEMP) which is funded by the European Union and the Free State of Saxony. Furthermore, the authors would like to acknowledge financial support from the Fraunhofer Attract program and the Friedrich-und-Elisabeth-Boysen-Stiftung.

References

[1] J. Castro, S.F. Santos, A.L.M. Costa, A.R. Yavari, W. Botta, F.T.T. Ishikawa, J. Alloys Compd. 376 (2004) 251–256.
[2] M. Dornheim, S. Doppiu, G. Barkhordarian, U. Boesenberg, T. Klassen, O. Gutfleisch, R. Bormann, Scripta Mater. 56 (2007) 841–846.
[3] M. Fichtner, Adv. Eng. Mater. 7 (2005) 443–455.
[4] S. Kwon, S. Baek, D.R. Mumm, S.-H. Hong, M. Song, Int. J. Hydrogen Energy 33 (2008) 4586–4592.
[5] A. Zaluska, L. Zaluski, J.O. Ström-Olsen, Appl. Phys. A 72 (2001) 157–165.
[6] Y. Chen, C.A.C. Sequeira, C. Chen, X. Wang, Q. Wang, Int. J. Hydrogen Energy 28 (2003) 329–333.
[7] S. Suda, Y. Komazaki, N. Kobayashi, J. Less Common Met. 89 (1983) 317–324.
[8] S. Mellouli, H. Dhaou, F. Askri, A. Jemni, S.B. Nasrallah, Int. J. Hydrogen Energy 34 (2009) 9393–9401.
[9] A. Chaise, P.D. Rango, P. Marty, D. Fruchart, S. Miraglia, R. Olivès, S. Garrier, Int. J. Hydrogen Energy 34 (2009) 8589–8596.
[10] K.J. Kim, M. Blanca, R. Arsenal, K.-H. Lee, Int. J. Hydrogen Energy 26 (2001) 609–613.
[11] H.P. Klein, M. Groll, Int. J. Hydrogen Energy 29 (2004) 1503–1511.
[12] A.R. Sánchez, H.-P. Klein, M. Groll, Int. J. Hydrogen Energy 28 (2003) 515–527.
[13] S. Kalinichenka, L. Röntzsch, B. Kieback, Int. J. Hydrogen Energy 34 (2009) 7749–7755.
[14] S. Kalinichenka, L. Röntzsch, C. Baehtz, B. Kieback, J. Alloys Compd. 496 (2010) 608–613.
[15] Z. Dehouche, R. Djaozandry, J. Goyette, T.K. Bose, J. Alloys Compd. 288 (1999) 269–276.
[16] G. Liang, J. Huot, S. Boily, A.V. Neste, R. Schulz, J. Alloys Compd. 292 (1999) 247–252.
[17] D. Vojtech, P. Novák, J. Cízkovský, V. Knotek, F. Prusa, J. Phys. Chem. Solids 68 (2007) 813–817.
[18] Y. Kaplan, Int. J. Hydrogen Energy 34 (2009) 2288–2294.
[19] B.D. MacDonald, A.M. Rowe, Int. J. Hydrogen Energy 31 (2006) 1721–1731.
[20] M. Melnichuk, G. Andreasen, H.L. Corso, A. Visintin, H.A. Peretti, Int. J. Hydrogen Energy 33 (2008) 3571–3575.
[21] P. Muthukumar, U. Madhavakrishna, A. Dewan, Int. J. Hydrogen Energy 32 (2007) 4988–4997.
[22] C. Pohlmann, L. Röntzsch, S. Kalinichenka, Th. Hutsch, B. Kieback, Int. J. Hydrogen Energy 35 (2010) 12829–12836.